Jpn J Ophthalmol
Vol 53: 297–314, 2009

References

1. Webb RH, Hughes GW. Scanning laser ophthalmoscope. IEEE Trans Biomed Eng 1981;28:488–492.
2. Mainster MA, Timberlake GT, Webb RH, Hughes GW. Scanning laser ophthalmoscopy. Clinical applications. Ophthalmology 1982;89:852–857.
3. Huang D, Swanson EA, Lin CP, et al. Optical coherence tomography. Science 1991;254:1178–1181.
4. Hee MR, Izatt JA, Swanson EA, et al. Optical coherence tomography of the human retina. Arch Ophthalmol 1995;113:325–332.
5. Rushton WA. The difference spectrum and the photosensitivity of rhodopsin in the living human eye. J Physiol 1956;134:11–29.
6. Hood C, Rushton WA. The Florida retinal densitometer. J Physiol 1971;217:213–229.
7. Rushton WA. Cone pigment kinetics in the protanope. J Physiol 1963;168:374–388.
8. Alpern M, Maaseidvaag F, Oba N. The kinetics of cone visual pigments in man. Vision Res 1971;11:539–549.
9. Alpern M. Rhodopsin kinetics in the human eye. J Physiol 1971;217:447–471.
10. van Norren D, van de Kraats J. Retinal densitometer with the size of a fundus camera. Vision Res 1989;29:369–374.
11. Kilbride PE, Read JS, Fishman GA, Fishman M. Determination of human cone pigment density difference spectra in spatially resolved regions of the fovea. Vision Res 1983;23:1341–1350.
12. Kilbride PE, Keehan KM. Visual pigments in the human macula assessed by imaging fundus reflectometry. Appl Opt 1990;29:1427–1435.
13. Faulkner DJ, Kemp CM. Human rhodopsin measurement using a T.V.-based imaging fundus reflectometer. Vision Res 1984;24:221–231.
14. Kemp CM, Faulkner DJ, Jacobson SG. The distribution and kinetics of visual pigments in the cat retina. Invest Ophthalmol Vis Sci 1988;29:1056–1065.
15. Kemp CM, Jacobson SG, Faulkner DJ. Two types of visual dysfunction in autosomal dominant retinitis pigmentosa. Invest Ophthalmol Vis Sci 1988;29:1235–1241.
16. van Norren D, van de Kraats J. Imaging retinal densitometry with a confocal scanning laser ophthalmoscope. Vis Res 1989;29:1825–1830.
17. Elsner AE, Burns SA, Hughes GW, Webb RH. Reflectometry with a scanning laser ophthalmoscope. Appl Opt 1992;31:3697–3710.
18. Elsner AE, Burns SA, Beausencourt E, Weiter JJ. Foveal cone photopigment distribution: small alterations associated with macular pigment distribution. Invest Ophthalmol Vis Sci 1998;39:2394–2404.
19. Zepeda A, Arias C, Sengpiel F. Optical imaging of intrinsic signals: recent developments in the methodology and its applications. J Neurosci Methods 2004;136:1–21.
20. Ts'o DY, Frostig RD, Lieke EE, Grinvald A. Functional organization of primate visual cortex revealed by high resolution optical imaging. Science 1990;249:417–420.
21. Frostig RD, Lieke EE, Ts'o DY, Grinvald A. Cortical functional architecture and local coupling between neuronal activity and the microcirculation revealed by in vivo high-resolution optical imaging of intrinsic signals. Proc Natl Acad Sci U S A 1990;87:6082–6086.
22. Roe AW, Ts'o DY. Visual topography in primate V2: multiple representation across functional stripes. J Neurosci 1995;15:3689–3715.
23. Ghose GM, Ts'o DY. Form processing modules in primate area V4. J Neurophysiol 1997;77:2191–2196.
24. Malonek D, Tootell RB, Grinvald A. Optical imaging reveals the functional architecture of neurons processing shape and motion in owl monkey area MT. Proc R Soc Lond B Biol Sci 1994;258:109–119.
25. Tsunoda K, Yamane Y, Nishizaki M, Tanifuji M. Complex objects are represented in macaque inferotemporal cortex by the combination of feature columns. Nat Neurosci 2001;4:832–838.
26. MacVicar BA, Hochman D. Imaging of synaptically evoked intrinsic optical signals in hippocampal slices. J Neurosci 1991;11:1458–1469.
27. Bonhoeffer T, Grinvald A. Optical imaging based on intrinsic signals: the methodology. In: Toga AW, Mazziotta JC, editors. Brain mapping. San Diego: Academic Press; 1996. p. 55–97.
28. Weliky M, Kandler K, Fitzpatrick D, Katz LC. Patterns of excitation and inhibition evoked by horizontal connections in visual cortex share a common relationship to orientation columns. Neuron 1995;15:541–552.
29. Das A, Gilbert CD. Long-range horizontal connections and their role in cortical reorganization revealed by optical recording of cat primary visual cortex. Nature 1995;375:780–784.
30. Tsunoda K, Oguchi Y, Hanazono G, Tanifuji M. Mapping cone- and rod-induced retinal responsiveness in macaque retina by optical imaging. Invest Ophthalmol Vis Sci 2004;45:3820–3826.
31. Crittin M, Riva CE. Functional imaging of the human papilla and peripapillary region based on flicker-induced reflectance changes. Neurosci Lett 2004;360:141–144.
32. Abramoff MD, Kwon YH, Ts'o D, et al. Visual stimulus-induced changes in human near-infrared fundus reflectance. Invest Ophthalmol Vis Sci 2006;47:715–721.
33. Grieve K, Roorda A. Intrinsic signals from human cone photoreceptors. Invest Ophthalmol Vis Sci 2008;49:713–719.
34. Nelson DA, Krupsky S, Pollack A, et al. Special report: noninvasive multi-parameter functional optical imaging of the eye. Ophthalmic Surg Lasers Imaging 2005;36:57–66.
35. Harary HH, Brown JE, Pinto LH. Rapid light-induced changes in near infrared transmission of rods in *Bufo marinus*. Science 1978;202:1083–1085.
36. Yao XC, Yamauchi A, Perry B, George JS. Rapid optical coherence tomography and recording functional scattering changes from activated frog retina. Appl Opt 2005;44:2019–2023.
37. Hanazono G, Tsunoda K, Shinoda K, Tsubota K, Miyake Y, Tanifuji M. Intrinsic signal imaging in macaque retina reveals different types of flash-induced light reflectance changes of different origins. Invest Ophthalmol Vis Sci 2007;48:2903–2912.
38. Inomata K, Tsunoda K, Hanazono G, et al. Distribution of retinal responses evoked by transscleral electrical stimulation detected by intrinsic signal imaging in macaque monkeys. Invest Ophthalmol Vis Sci 2008;49:2193–2200.
39. Hanazono G, Tsunoda K, Kazato Y, Tsubota K, Tanifuji M. Evaluating neural activity of retinal ganglion cells by flash-evoked intrinsic signal imaging in macaque retina. Invest Ophthalmol Vis Sci 2008;49:4655–4663.
40. Wali N, Leguire LE. The photopic hill: a new phenomenon of the light adapted electroretinogram. Doc Ophthalmol 1992;80:335–345.
41. Wagman IH, Waldman J, Naidoff D, Feinschil LB, Cahan R. The recording of the electroretinogram in humans and in animals; investigation of retinal sensitivity following brief flashes of light. Am J Ophthalmol 1954;38:60–69.
42. Mahroo OA, Lamb TD. Recovery of the human photopic electroretinogram after bleaching exposures: estimation of pigment regeneration kinetics. J Physiol 2004;554:417–437.
43. Weinhaus RS, Burke JM, Delori FC, Snodderly DM. Comparison of fluorescein angiography with microvascular anatomy of macaque retinas. Exp Eye Res 1995;61:1–16.
44. Roy C, Sherrington C. On the regulation of the blood supply of the brain. J Physiol 1890;11:85–108.
45. Villringer A, Dirnagl U. Coupling of brain activity and cerebral blood flow: basis of functional neuroimaging. Cerebrovasc Brain Metab Rev 1995;7:240–276.
46. Bizheva K, Pflug R, Hermann B, et al. Optophysiology: depth-resolved probing of retinal physiology with functional ultrahigh-resolution optical coherence tomography. Proc Natl Acad Sci U S A 2006;103:5066–5071.

47. Dawson WW, Trick GL, Litzkow CA. Improved electrode for electroretinography. Invest Ophthalmol Vis Sci 1979;18:988–991.
48. Gekeler F, Messias A, Ottinger M, Bartz-Schmidt KU, Zrenner E. Phosphenes electrically evoked with DTL electrodes: a study in patients with retinitis pigmentosa, glaucoma, and homonymous visual field loss and normal subjects. Invest Ophthalmol Vis Sci 2006;47:4966–4974.
49. Crapper DR, Noell WK. Retinal excitation and inhibition from direct electrical stimulation. J Neurophysiol 1963;26:924–947.
50. Knighton RW. An electrically evoked slow potential of the frog's retina. I. Properties of response. J Neurophysiol 1975;38:185–197.
51. Stett A, Barth W, Weiss S, Haemmerle H, Zrenner E. Electrical multisite stimulation of the isolated chicken retina. Vision Res 2000;40:1785–1795.
52. Kaneko A, Saito T. Ionic mechanisms underlying the responses of off-center bipolar cells in the carp retina. II. Studies on responses evoked by transretinal current stimulation. J Gen Physiol 1983;81:603–612.
53. Toyoda J, Fujimoto M. Application of transretinal current stimulation for the study of bipolar-amacrine transmission. J Gen Physiol 1984;84:915–925.
54. Shimazu K, Miyake Y, Watanabe S. Retinal ganglion cell response properties in the transcorneal electrically evoked response of the visual system. Vision Res 1999;39:2251–2260.
55. Margalit E, Thoreson WB. Inner retinal mechanisms engaged by retinal electrical stimulation. Invest Ophthalmol Vis Sci 2006; 47:2606–2612.
56. Byzov AL, Trifonov JA. The response to electric stimulation of horizontal cells in the carp retina. Vis Res 1968;8:817–822.
57. Murakami M, Takahashi K. Calcium action potential and its use for measurement of reversal potentials of horizontal cell responses in carp retina. J Physiol 1987;386:165–180.
58. Takahashi K, Murakami M. Calcium action potential in ON–OFF transient amacrine cell of the carp retina. Brain Res 1988; 456:29–37.
59. Li L, Hayashida Y, Yagi T. Temporal properties of retinal ganglion cell responses to local transretinal current stimuli in the frog retina. Vis Res 2005;45:263–273.
60. Potts AM, Inoue J, Buffum D. The electrically evoked response of the visual system (EER). Invest Ophthalmol 1968;7:269–278.
61. Potts AM, Inoue J. The electrically evoked response (EER) of the visual system. II. Effect of adaptation and retinitis pigmentosa. Invest Ophthalmol 1969;8:605–612.
62. Potts AM, Inoue J. The electrically evoked response of the visual system (EER). 3. Further contribution to the origin of the EER. Invest Ophthalmol 1970;9:814–819.
63. Miyake Y, Yanagida K, Yagasaki K. Clinical application of EER (electrically evoked response). 1. Analysis of EER in normal subjects [in Japanese]. Nippon Ganka Gakkai Zasshi 1980;84: 354–360.
64. Miyake Y, Yanagida K, Yagasaki K. Clinical application of EER (electrically evoked response). 2. Analysis of EER in patients with dysfunctional rod or cone visual pathway [in Japanese]. Nippon Ganka Gakkai Zasshi 1980;84:502–509.
65. Miyake Y, Yanagida K, Yagasaki K. Clinical application of EER (electrically evoked response). 3. Analysis of EER in patients with central retinal arterial occlusion [in Japanese]. Nippon Ganka Gakkai Zasshi 1980;84:587–593.
66. Miyake Y, Yanagida K, Yagasaki K. Clinical application of EER (electrically evoked response). Analysis of EER in patients with optic nerve disease [in Japanese]. Nippon Ganka Gakkai Zasshi 1980;84:2047–2052.
67. Brindley GS. The site of electrical excitation of the human eye. J Physiol 1955;127:189–200.
68. Toi VV, Riva CE. Variations of blood flow at optic disc nerve head induced by sinusoidal flicker stimulation in cats. J Physiol 1994;482:189–202.
69. Falsini B, Riva CE, Logean E. Flicker-evoked changes in human optic nerve blood flow: relationship with retinal neural activity. Invest Ophthalmol Vis Sci 2002;43:2309–2316.
70. Riva CE, Logean E, Falsini B. Temporal dynamics and magnitude of the blood flow response at the optic disk in normal subjects during functional retinal flicker-stimulation. Neurosci Lett 2004; 356:75–78.
71. Riva CE, Salgarello T, Logean E, Colotto A, Galan EM, Falsini B. Flicker-evoked response measured at the optic disc rim is reduced in ocular hypertension and early glaucoma. Invest Ophthalmol Vis Sci 2004;45:3662–3668.
72. Kelly DH. Visual response to time-dependent stimuli. I. Amplitude sensitivity measurements. J Opt Soc Am 1961;51:422–429.
73. Gebhard JW. Thresholds of the human eye for electric stimulation by different wave forms. J Exp Psychol 1952;44:132–140.
74. Regan D. A high frequency mechanism which underlies visual evoked potentials. Electroencephalogr Clin Neurophysiol 1968;25: 231–237.
75. Tanino T, Kato S, Kawasumi M. Studies on electrically evoked pupillary reflex—indirect reflex and its frequency characteristic. Jpn J Ophthalmol 1981;25:423–429.
76. Malonek D, Grinvald A. Interactions between electrical activity and cortical microcirculation revealed by imaging spectroscopy: implications for functional brain mapping. Science 1996;272: 551–554.
77. Pouratian N, Toga A. Optical imaging based on intrinsic signals. In: Toga AW, Mazziotta JC, editors. Brain mapping. San Diego: Academic Press; 2002. p. 97–140.
78. Barriga ES, Pattichis M, Ts'o D, et al. Spatiotemporal independent component analysis for the detection of functional responses in cat retinal images. IEEE Trans Med Imaging 2007; 26:1035–1045.
79. Fukuda M, Rajagopalan UM, Homma R, Matsumoto M, Nishizaki M, Tanifuji M. Localization of activity-dependent changes in blood volume to submillimeter-scale functional domains in cat visual cortex. Cereb Cortex 2005;15:823–833.
80. Longo A, Geiser M, Riva CE. Subfoveal choroidal blood flow in response to light–dark exposure. Invest Ophthalmol Vis Sci 2000;41:2678–2683.
81. Riva CE, Harino S, Shonat RD, Petrig BL. Flicker evoked increase in optic nerve head blood flow in anesthetized cats. Neurosci Lett 1991;128:291–296.
82. Riva CE, Falsini B, Logean E. Flicker-evoked responses of human optic nerve head blood flow: luminance versus chromatic modulation. Invest Ophthalmol Vis Sci 2001;42:756–762.
83. Viswanathan S, Frishman LJ, Robson JG, Harwerth RS, Smith EL 3rd. The photopic negative response of the macaque electroretinogram: reduction by experimental glaucoma. Invest Ophthalmol Vis Sci 1999;40:1124–1136.
84. Viswanathan S, Frishman LJ, Robson JG, Walters JW. The photopic negative response of the flash electroretinogram in primary open angle glaucoma. Invest Ophthalmol Vis Sci 2001;42:514–522.
85. Narahashi T. Chemicals as tools in the study of excitable membranes. Physiol Rev 1974;54:813–889.
86. Bloomfield SA. Effect of spike blockade on the receptive-field size of amacrine and ganglion cells in the rabbit retina. J Neurophysiol 1996;75:1878–1893.
87. Quigley HA, Green WR. The histology of human glaucoma cupping and optic nerve damage: clinicopathologic correlation in 21 eyes. Ophthalmology 1979;86:1803–1830.
88. Quigley HA, Addicks EM, Green WR. Optic nerve damage in human glaucoma. III. Quantitative correlation of nerve fiber loss and visual field defect in glaucoma, ischemic neuropathy, papilledema, and toxic neuropathy. Arch Ophthalmol 1982;100: 135–146.
89. Quigley HA, Dunkelberger GR, Green WR. Retinal ganglion cell atrophy correlated with automated perimetry in human eyes with glaucoma. Am J Ophthalmol 1989;107:453–464.

90. Glovinsky Y, Quigley HA, Dunkelberger GR. Retinal ganglion cell loss is size dependent in experimental glaucoma. Invest Ophthalmol Vis Sci 1991;32:484–491.
91. Frishman LJ, Shen FF, Du L, et al. The scotopic electroretinogram of macaque after retinal ganglion cell loss from experimental glaucoma. Invest Ophthalmol Vis Sci 1996;37:125–141.
92. Kerrigan-Baumrind LA, Quigley HA, Pease ME, Kerrigan DF, Mitchell RS. Number of ganglion cells in glaucoma eyes compared with threshold visual field tests in the same persons. Invest Ophthalmol Vis Sci 2000;41:741–748.
93. Mcilwain JT. Receptive fields of optic tract axons and lateral geniculate cells: peripheral extent and barbiturate sensitivity. J Neurophysiol 1964;27:1154–1173.
94. Mcilwain JT. Some evidence concerning physiological basis of periphery effect in cats retina. Exp Brain Res 1966;1:265–271.
95. Derrington AM, Lennie P, Wright MJ. Mechanism of peripherally evoked-responses in retinal ganglion-cells. J Physiol 1979;289: 299–310.
96. Toth LJ, Rao SC, Kim DS, Somers D, Sur M. Subthreshold facilitation and suppression in primary visual cortex revealed by intrinsic signal imaging. Proc Natl Acad Sci U S A 1996;93:9869–9874.
97. Kaplan E, Benardete E. The dynamics of primate retinal ganglion cells. Prog Brain Res 2001;134:17–34.
98. Yao XC, Zhao YB. Optical dissection of stimulus-evoked retinal activation. Opt Exp 2008;16:12446–12459.
99. Zhao YB, Yao XC. Intrinsic optical imaging of stimulus-modulated physiological responses in amphibian retina. Opt Lett 2008;33:342–344.
100. Srinivasan VJ, Wojtkowski M, Fujimoto JG, Duker JS. In vivo measurement of retinal physiology with high-speed ultrahigh-resolution optical coherence tomography. Opt Lett 2006;31: 2308–2310.

Stargardt Disease with Preserved Vision Accompanied by Foveal Retinal Pigment Epithelium Hypertrophy

Kaoru Fujinami[1, 2], MD, Masakazu Akahori[2], PhD, Masaki Fukui[1], MD, Kazushige Tsunoda[1], MD, Takeshi Iwata[2], PhD and Yozo Miyake[1, 3], MD

[1]Laboratory of Visual Physiology, National Institute of Sensory Organs, 2-5-1 Higashigaoka, Meguro-ku, Tokyo 152-8902, Japan

[2] Division of Molecular & Cellular Biology, National Institute of Sensory Organs, National Hospital Organization, Tokyo Medical Center, 2-5-1 Higashigaoka, Meguro-ku, Tokyo 152-8902, Japan

[3]Aichi Shukutoku University, Aichi, Japan, 9, Nagakute Katahira, Nagakute-cho, Aichi-gun, Aichi, 480-1197, Japan

Running head: Stargardt Disease with RPE Hypertrophy

Corresponding author: Kazushige Tsunoda, M.D., Laboratory of Visual Physiology, National Institute of Sensory Organs, 2-5-1 Higashigaoka, Meguro-ku, Tokyo 152-8902, Japan

TEL: +81-3-3411-0111 ext 6615

FAX: +81-3-3412-9811

E-mail: tsunodakazushige@kankakuki.go.jp

Key Words: Stargardt disease, Retinal pigment epithelium hypertrophy, ATP-binding cassette transporter gene, Heterozygous mutation

Stargardt disease (STGD) has a juvenile to young-adult onset, a rapid decrease of central vision, and progressive bilateral atrophy of the sensory central retina and foveal retinal pigment epithelium (RPE). Yellow-orange flecks are often detected around the macula and/or the midretina. (Rotenstreich et al. 2003) Mutations in the gene encoding the ATP-binding cassette transporter gene (ABCA4) are responsible for autosomal recessive STGD. (Allikmets 1997; Webster et al. 2001) We examined a patient who had the characteristic signs of STGD but had good visual acuity and RPE hypertrophy.

A 66-year-old man complained of photophobia and a paracentral scotoma which was present since his teens and had not worsened. None of his family members had complained of the same symptoms. His visual acuity was 20/15 OU, and ophthalmoscopy identified a dark brown, well demarcated area of RPE hypertrophy at the fovea surrounded by RPE atrophy and flecks in the macula (Figure 1). Fluorescein angiograms showed blockage of the choriocapillaris in the foveal area, window defect at the flecks, and a dark choroid. The optical coherence tomographic (OCT) images showed a well-preserved sensory retina and RPE hypertrophy at the fovea, which was surrounded by atrophic sensory retina and underlying atrophic RPE. Functional analysis (statistic visual field perimetry and focal macular electroretinograms) also demonstrated a well-preserved retina at the fovea. Genetic analysis with direct DNA

sequencing of amplified products revealed four reported polymorphisms (Allikmets 1997; Briggs et al. 2001; Webster et al. 2001) and one new mutation, Met280Thr, in exon 7 of the ABCA4 gene (Table 1).

Our patient had a stationary clinical course and other clinical findings that were pathognomonic of typical STGD. However, he had 20/15 vision and well-preserved foveal function. To the best of our knowledge, this is the first report of a patient with STGD with good vision and foveal RPE hypertrophy, although Rotenstreich et al reported that 39% of STGD patients who were > 61-years-of-age had visual acuity of 20/40 or better. (Rotenstreich et al. 2003) Both the morphological and functional assessments supported the good foveal function. The OCT images also showed that the area of RPE hypertrophy corresponded with the area of preserved sensory retina. We suggest that the well-preserved foveal function in our case may be because of the RPE hypertrophy, although it is not clear whether the hypertrophy was congenital or secondary to the photoreceptor damage.

The inheritance of STGD is autosomal recessive, however our patient had four polymorphisms and one heterozygous gene mutation c.839T>C in exon 7 in the ABCA4 gene. This mutation causes an amino acid substitution of Met280Thr. Although patients with heterozygous mutations have also been reported in patients with STGD, their ages

at onset with which the severity of STGD is correlated were not necessarily late.(Lewis et al. 1999) Little is known about how the heterozygous mutation is expressed in this unique phenotype. The new mutation in our patient was located outside the known functional domains of ATP-binding or transmembrane site, (Lewis et al. 1999) which may explain the mild effect of the missense mutation. We should also consider a modifier gene effect in our patient.

Although the relationship between the new mutation of the ABCA4 gene and RPE hypertrophy is unclear, the unique phenotype and genotype of our patient may give additional information on the mechanism of photoreceptor degeneration in eyes with STGD.

References

Allikmets R (1997): A photoreceptor cell-specific ATP-binding transporter gene (ABCR) is mutated in recessive Stargardt macular dystrophy. Nat Genet 17: 122.

Briggs CE, D Rucinski, PJ Rosenfeld, T Hirose, EL Berson & TP Dryja (2001): Mutations in ABCR (ABCA4) in patients with Stargardt macular degeneration or cone-rod degeneration. Invest Ophthalmol Vis Sci 42: 2229-36.

Lewis RA, NF Shroyer, N Singh, R Allikmets, A Hutchinson, Y Li, JR Lupski, M Leppert & M Dean (1999): Genotype/Phenotype analysis of a photoreceptor-specific ATP-binding cassette transporter gene, ABCR, in Stargardt disease. Am J Hum Genet 64: 422-34.

Rotenstreich Y, GA Fishman & RJ Anderson (2003): Visual acuity loss and clinical observations in a large series of patients with Stargardt disease. Ophthalmology 110: 1151-8.

Webster AR, E Heon, AJ Lotery, K Vandenburgh, TL Casavant, KT Oh, G Beck, GA Fishman, BL Lam, A Levin, JR Heckenlively, SG Jacobson, RG Weleber, VC Sheffield & EM Stone (2001): An analysis of allelic variation in the ABCA4 gene. Invest Ophthalmol Vis Sci 42: 1179-89.

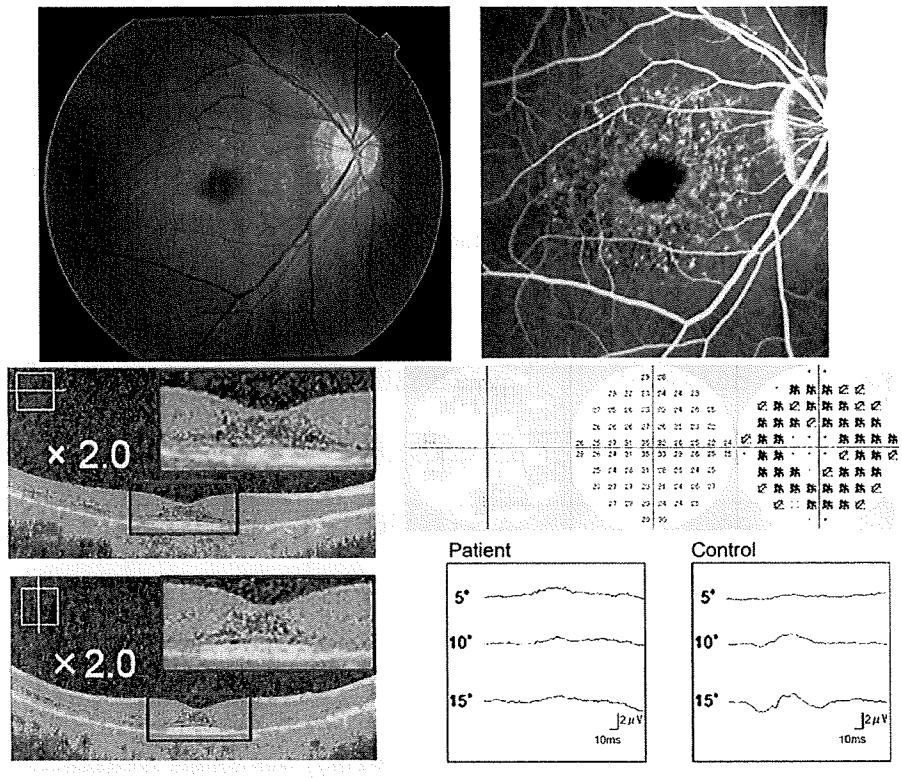

Figure Legends

Figure 1. Fundus photograph, fluorescein angiogram (FA), optical coherence tomography (OCT), Humphrey statistic perimetry, and focal macular electroretinograms (FMERGs) of an eye of a patient with Stargardt disease.

Top left: Fundus photograph showing dark brown, well demarcated area in the fovea surrounded by orange-yellow flecks in the macula.

Top right: FA showing blockage in the foveal area, ring-shaped mottled hyperfluorescence in the macula, and 'dark choroid.'

Middle left and Bottom left: OCT images (middle; horizontal, bottom; vertical) showing preserved sensory retina and thickened retinal pigment epithelium (RPE) layer in the fovea. In the juxta-foveal region, the atrophy of both sensory retina and RPE can be seen. The extended images within the red lines are attached.

Middle right: Humphrey statistic perimetry showing ring-shaped paracentral scotoma (10-2 strategy).

Bottom right: FMERGs showing a normal response elicited by a 5-degree stimulus spot and reduced responses elicited by 10-degree and 15-degree spots.

90x90mm (500 x 500 DPI)

Table 1 ABCA4 GENE MUTATION AND Polymorphisms				
Exon	Nucleotide Change	Effect Changes	Het / Hom	References
Mutation				
7	c.839T>C	p.Met280Thr	Het	Present study
Polymorphisms				
10	c.1269C>T	p.His424His	Hom	[3]
45	c.6249C>T	p.Ile2083Ile	Het	[2]
46	c.6285T>C	p.Asp2095Asp	Het	[4]
49	c.6764G>T	p.Ser2255Ile	Het	[2]

The translational start codon ATG/methionine is numbered as +1. One novel disease-associated mutation [c.839T>C (p.Met280Thr)] was found. References of previously reported polymorphisms are indicated.

Het, heterozygote; Hom, homozygote.

Chapter 5
How Images of Objects Are Represented in Macaque Inferotemporal Cortex

Manabu Tanifuji, Takayuki Sato, Go Uchida, Yukako Yamane, and Kazushige Tsunoda

Abstract Visual object recognition is a simple and easy task in our daily life. However, the mechanisms for recognizing objects are not at all simple nor easy. To understand neural mechanisms of object recognition, we have investigated representation of object images in macaque inferior temporal cortex that is the area essential for object recognition. Optical intrinsic signal imaging has revealed that object images are represented by the combinatorial code at the columnar level, where each column represents a visual feature of object images. The visual features represented by columns include local features as well as global features representing spatial arrangements of local features. Here, columns are supposed to be functional units for object representation. However, difference in object selectivity among nearby cells does not support the concept of columns as the functional units. Quantitative analysis of object responses of single cells and population activity revealed that each cell in a columnar region is characterized by cell specific property and property common across the cells in the columnar region, suggesting two different levels (single cell and columnar level) of object representation. Possible role of these two levels of object representation will be discussed.

5.1 Introduction

In order to understand neural mechanisms of object recognition, we have investigated representation of object images in inferotemporal (IT) cortex of macaque monkeys. This area of brain is essential for the recognition of objects by their visual images, and neurons in this area are known to respond to images of complex objects (Gross 1994; Gross et al. 1979; Desimone et al. 1984; Bruce et al. 1981; Perrett

M. Tanifuji (✉)
Laboratory for Integrative Neural Systems, RIKEN Brain Science Institute, Wako, Saitama, 351-0198, Japan
e-mail: tanifuji@riken.go.jp

A.W. Roe (ed.), *Imaging the Brain with Optical Methods*,
DOI 10.1007/978-1-4419-0452-2_5,

et al. 1982; Tanaka et al. 1991). Although some of these neurons specifically respond to certain objects such as faces, many IT neurons also well respond to visual features that are less complex than object images (Desimone et al. 1984; Bruce et al. 1981; Perrett et al. 1982; Tanaka et al. 1991). Since none of these visual features are specific enough, object representation takes the combined activation of multiple neurons to represent a particular object image in IT cortex. Investigations of object representation require analyses of activities of multiple neurons evoked by an object image.

Neurons responding to particular objects or visual features are not randomly distributed in IT cortex. Tanaka and colleagues found that neurons tuned to similar features were clustered together and formed a column in IT cortex (Feature column) (Fujita et al. 1992). Optical intrinsic signal imaging (OISI), that has columnar level resolution, is an appropriate technique to investigate object representation with multiple neurons (Grinvald et al. 1999). In fact, OISI revealed that an object image activates multiple spots (activity spots) in IT cortex, and that distribution patterns of activity spots are different from object to object (Tsunoda et al. 2001; Yamane et al. 2006). In this chapter, we present our studies with OISI that revealed what and how activity spots (corresponding to feature columns) are used to represent object images in IT cortex (Tsunoda et al. 2001; Yamane et al. 2006; Wang et al. 1996; Wang et al. 1998).

OISI is still limited in spatial resolution. It does not allow us to resolve visual responses at a level of single cells. Strictly speaking, object representation revealed by OISI is at the level of columns, and, in principle, columnar level representation could be different from representation at the level of single cells. In addition, recent studies have reported that object selectivity of nearby cells is largely different; these observations seemingly contradict to the column hypothesis (Tamura et al. 2005; Kreiman et al. 2006; Sato et al. 2009). Our recent study suggests that this apparent contradiction is due to the response property specific to neurons that obscure the response property common across the cells in a columnar region (Sato et al. 2009). The critical question is how to relate object representation at columnar level and a possible representation by combinations of activities of single cells in close vicinity. In the last part of the chapter, we discuss this issue. The above study also suggests that, in contrast to the columnar organizations in V1, the columnar structure in IT cortex may not uniformly cover entire IT (Sato et al. 2009).

IT cortex is subdivided into multiple areas. Our investigations focus on dorsal part of area TEa, that is the most anterior part of IT cortex where OISI is still applicable. Furthermore, the results shown here were based on the experiments with anesthetized monkeys. Thus, we cannot directly relate object representation observed in our studies to recognition in waking animals, but studies with anesthetized animals have an advantage that they can reveal object representation unbiased toward particular behavioral contexts.

To begin with, basic characteristics of intrinsic signals in IT cortex and physiological studies related to the columnar organizations are briefly reviewed, since studies on these two issues provide basis for our studies with OISI.

5.2 Optical Intrinsic Signal Imaging (OISI) in IT Cortex

Activation of neurons elicits changes in reflection of light from neural tissues. The changes (intrinsic signals) reflect three secondary physiological mechanisms associated with neural activation: deoxygenation level of hemoglobin (Vanzetta and Grinvald 1999), blood volume changes in capillaries (Fukuda et al. 2005; Vanzetta et al. 2004), and microscopic changes in tissue structure that cause changes in light scattering (MacVicar and Hockman 1991; Tsunoda et al. 2004). Relative contribution of these three components to intrinsic signals depends on the wavelength of light used for illuminating the cortex. In OISI from area TE, we used wavelengths at around 610 nm, where deoxygenation of hemoglobin is the dominant component. The typical time courses of the signals were not very different from those in V1: the signals reached a peak of increase in absorption at about 1–2 s after the stimulus onset, crossed the baseline absorption level at around 2–4 s. after the stimulus onset, and then showed absorption decreases that lasted for several seconds (Fig. 5.1). The initial increase in absorption corresponds to deoxyhemoglobin increase due to oxygen consumption by neurons activated by the stimulus and late decrease in absorption corresponds to replacement of deoxyhemoglobin with oxyhemoglobin due to increased blood flow triggered by the neural activation.

To obtain spatial patterns of intrinsic signals in area TE, we took images of cortical surface during 2.5 s period starting from 0.5 s after the stimulus onset by a CCD

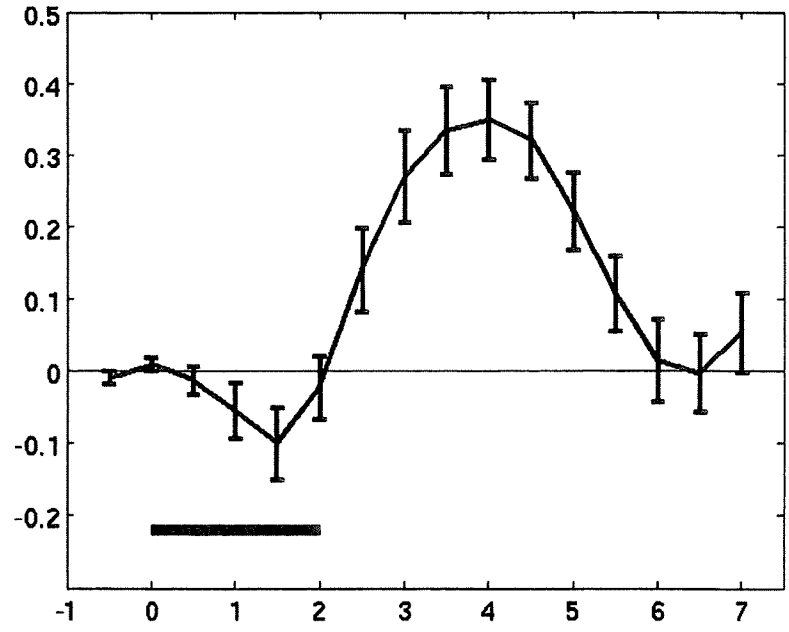

Fig. 5.1 The time course of intrinsic signals in area TE. Horizontal and vertical axes represent time (s) and reflection changes (%), respectively. *Horizontal bar*, the period for visual stimulation

camera, averaged them, and subtracted an image taken just before the stimulus onset from the averaged image (Tsunoda et al. 2001; Yamane et al. 2006). Thus, spatial patterns of intrinsic signals in area TE mainly reflect deoxygenation of hemoglobin induced by increased neural activity. Though OISI is typically used to visualize activation at the level of columns, raw intrinsic signals were not confined to columnar regions (global signals) (Fig. 5.2c). The global signals were, however, locally modulated. The local peaks of modulation (activity spots) were extracted by removing a low spatial frequency component of intrinsic signals (filtered image, Fig. 5.2d). Activity spots were then demarcated by drawing contours crossing half height between peak absorption of the spot and background in the filtered image (Fig. 5.2b). The magnitudes of the absorption changes in the filtered intrinsic signals were well correlated with the average of multi-unit activities (avgMUA) recorded from the same spot. For eleven activity spots, for example, the mean and standard deviation of correlation coefficient was 0.61 ± 0.17, and this value is statistically significant ($p < 0.05$). As shown later, avgMUA gives a good estimate of the neural activity at the columnar level. Thus, the high spatial frequency component

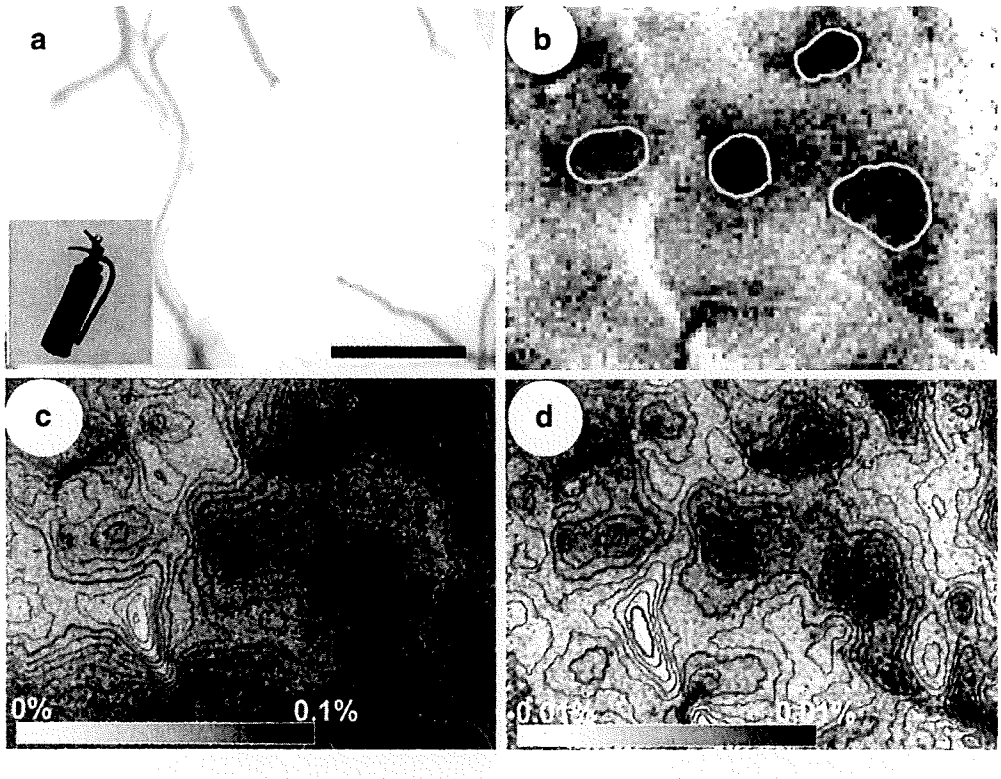

Fig. 5.2 A spatial pattern of intrinsic signals in IT. (**a**) Surface view of the exposed portion of IT cortex. Scale bar, 1 mm. (**b**) Activity spots outlined at the level of half the peak absorption value. (**c**) the spatial pattern of raw intrinsic signals without filtering. (**d**) spatial pattern of activity spots obtained by filtering raw intrinsic signals Scale bars in (**c**) and (**d**), percent changes in absorption increase. (modified from Tsunoda et al. (2001))

of intrinsic signals as in Fig 5.2b,d is in a good agreement with firing activity of population of neurons as seen in intrinsic signals in V1.

What about the low spatial frequency component of the raw intrinsic signals indicates? One possibility is that this low spatial frequency component (global signals) reflects synaptic potentials elicited by visual stimuli. To examine this possibility, we stained the cortex with the voltage sensitive dye RH1692 and compared the dye signal with intrinsic signals recorded from the same region (Homma and Tanifuji 2003). It is known that the voltage sensitive dye stains cellular membrane and that changes in flourescence of the dye reflect synaptic potentials rather than spiking activities (Grinvald et al. 1999). We found that the dye signals also revealed low and high spatial components, and local peaks of the dye signal coincide well with activity spots revealed by OISI. Since the low spatial frequency component of voltage sensitive dye signals was similar to that of the intrinsic signals, we think that raw intrinsic signals may also reflect synaptic potentials, and that intrinsic signals outside of the regions of activity spots reflect synaptic potentials below the threshold of neuronal firing. Similar argument was made for the global and local modulation of intrinsic signals observed in cat striate cortex (Das and Gilbert 1995). Interestingly, the low spatial frequency component is not uniformly distributed in space. For example, more absorption is seen in the right half than in the left half (Fig. 5.2c). Similar regional specificity was also observed in activation patterns recorded by voltage sensitive dye imaging with various object images. In this way, the distribution of the low frequency components was stimulus dependent. Some representations of object images may exist at the level of synaptic potentials as well as those at columnar levels.

5.3 Evidence for the Columnar Organization with Respect to the Critical Features in Area TE

Columnar organizations in the area TE were systematically investigated by Tanaka and colleagues (Tanaka et al. 1991; Fujita et al. 1992). They first determined a visual feature critical for each cell (Tanaka et al. 1991), and then investigated columnar organizations with respect to the critical features (Fujita et al. 1992). Here, the critical feature for a cell means the simplest visual feature that activates the cell equally well as the best object stimulus. To find such a critical feature, first, they searched for the most effective stimulus for each cell among more than a hundred of three-dimensional object stimuli. These stimuli included stuffed animals, plastic fruits and vegetables, and experimenter's hand and body. These stimuli were presented to the monkeys from various viewpoints to maximize the chance of finding the most effective image. Then, they generated modifications of the most effective stimulus and examined responses evoked by the simplified stimuli. If the cell responded to one of the simplified stimuli equally well as the original object stimulus, this new stimulus was further simplified. This procedure was repeated until the experimenter could not simplify the stimulus without significant reduction of the

evoked responses. Figure 5.3 shows a representative case of the stimulus simplification procedure according to their method, where we found a combination of the circle and rectangle was essential for the maximal activation of a cell. This cell was recorded from the activity spot that was expected to represent spatial relationship among object parts (discussed later in detail).

Tanaka and colleagues examined many TE neurons in this way and identified visual features essential for activating individual cells (Tanaka et al. 1991; Kobatake and Tanaka 1994). Many of these features are the combinations of simple shapes,

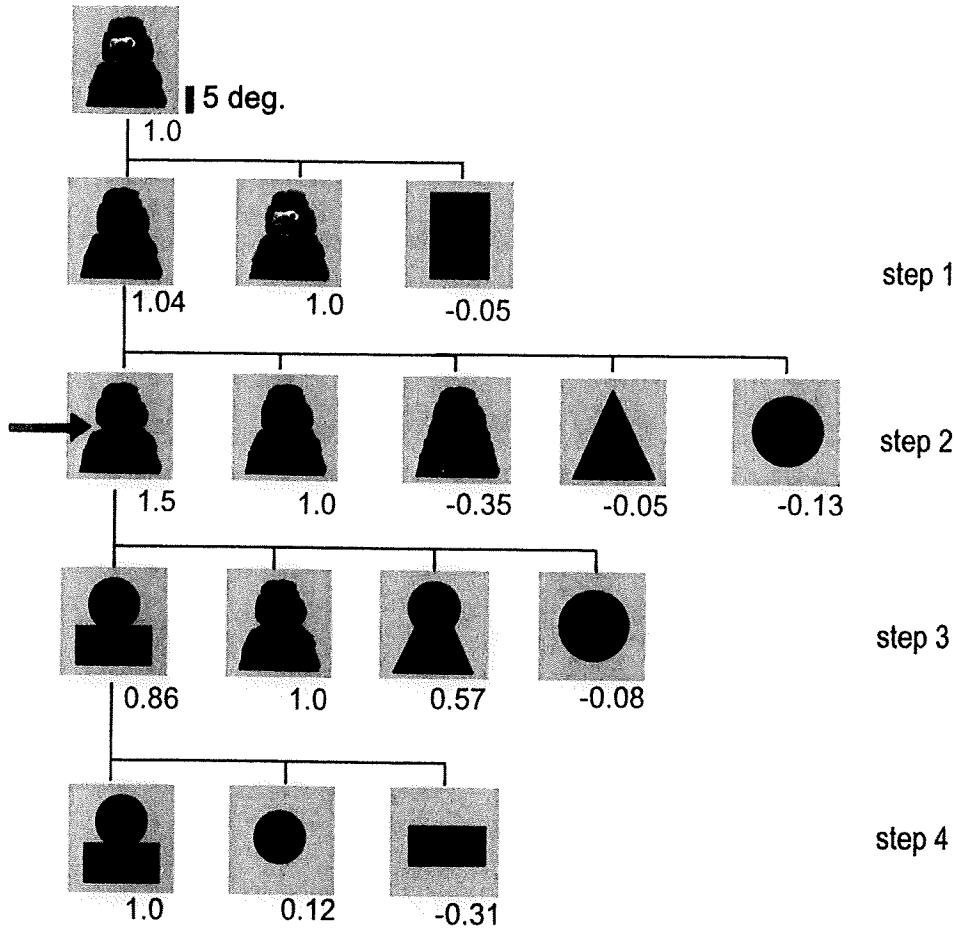

Fig. 5.3 Systematic stimulus simplification of an object image. The most effective object stimulus (*top* picture) was simplified step by step to determine the simplest stimulus that maximally activates the cell. Step 1 shows that neuronal activity elicited by the most effective object and its silhouettes are the same. The number below each picture indicates the response amplitudes normalized to the response to the reference stimulus. Step 2 examines the effect of the "sharpness" of the corner at the junction of the *upper* and *lower* parts (*arrow*) and shows that the silhouette with the sharpest corners (*leftmost* picture) is the most effective stimulus. Step 3 shows that activities elicited by the two *leftmost* stimuli are not significantly different. Step 4 shows that neither the *upper* nor *lower* part activates the cell. In this case, the critical feature was determined as the combination of a circle and a rectangle (*leftmost* picture in step 4). (Modified from Yamane et al. (2006))

colors, luminance gradient/contrast, and textures. These features are more complex than the optimal visual stimuli for cells in areas V1, V2, and V4, but still less complex than natural objects (Kobatake and Tanaka 1994).

Fujita et al. (1992) systematically examined the columnar organization in the area TE with respect to the critical features. First, they penetrated electrodes perpendicular to the cortical surface and determined a critical feature of one neuron within the track. Then, they prepared a set of visual stimuli including this critical feature and its modifications and examined the response selectivity of other neurons within the track using the set of visual stimuli. This experiment showed that the most effective stimulus for the cells in the track is the critical feature or visual features similar to it. They also examined neuronal responses along a tangential electrode penetration and found that neurons with similar responsiveness were localized within the range about 0.4 mm along the tangential track. These results suggest a columnar organization in the IT cortex with respect to the critical features of the cells. However, we often encounter nearby cells spaced only for about 150 μm apart but having different selectivity for object images. We will discuss later in this chapter what makes this difference in the selectivity of the critical features and object images.

Many investigations suggest that neurons in IT cortex were plastic. For example, the above group trained monkeys for a specific set of visual stimuli with a delayed match-to-sample task (Kobatake et al. 1998). They found that, compared with naïve monkeys, IT cortex of the trained monkeys contained more neurons tuned to a trained stimulus: the response to the best of the trained stimuli was higher than the responses to any other object images. Because we cannot keep tracking responses of a single neuron during training that takes more than a month, these results may not indicate that training changed visual responses of IT cells. Neurons that were previously not visually driven may turn out to be responsive to the trained stimulus. In either case, the columnar organization in IT cortex, if it exists, seems not static but could be modified by extensive experience of the monkeys.

5.4 Object Representation by Combinations of Activity Spots in Area TE

OISI revealed that an object image activates multiple activity spots (Figs. 5.2 and 5.4). The spatial patterns of these activity spots are different from object to object. Some of the spots were co-activated by different objects, while other spots were activated only by one object (Fig. 5.4a, b). Assuming that each spot represents a visual feature, activation of the spots specific to a single object is likely to indicate that the other objects lack the visual-feature represented by these spots. For example, the spots only activated by stimulus 1 may be related to horizontal red/blue stripes only seen in stimulus 1 (Fig. 5.4b). Comparison between the distribution patterns of activity spots and those produced by systematically simplified stimuli revealed that this was indeed the case (Fig. 5.4c). Here, a "black cat" (c-**1**) was

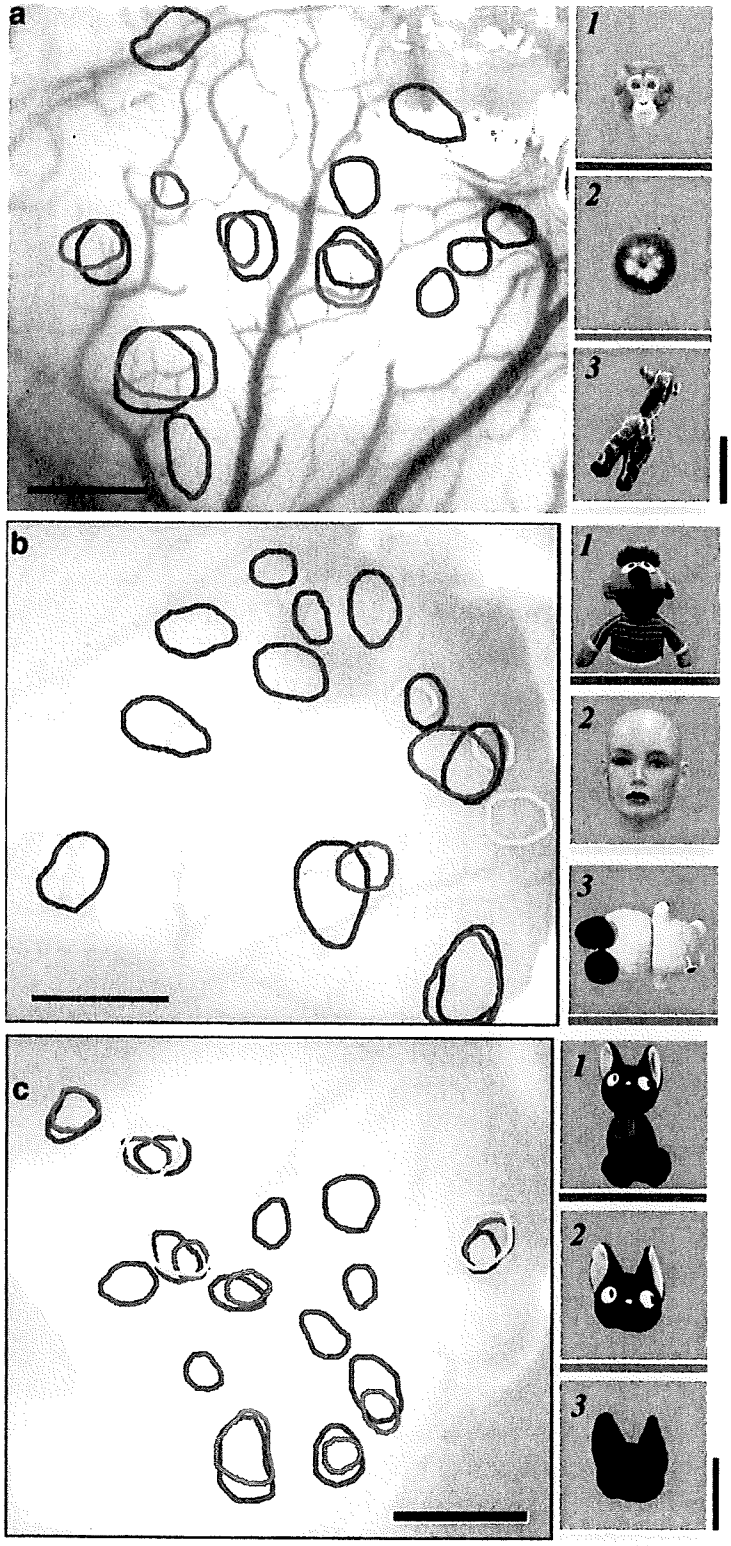

Fig. 5.4 Distribution of activity spots elicited by various object images (**a**,**b**) and simplified images (**c**). Contours of the activity spots were drawn as in Fig. 5.2. Horizontal scale bars, 1.0 mm. Vertical scale bars, 10°. (Modified from Tsunoda et al. (2001))

simplified to the "head" (c-**2**), and then to the "silhouette of the head" (c-**3**). The original image (c-**1**) elicited 14 spots, but presenting the "head" (c-**2**) elicited only eight spots of the original fourteen. The "silhouette" (c-**3**) only activated three (arrows) of the eight spots elicited by the "head" (c-**2**). Simplified stimuli lacking some of the visual features of the original image activated only a subset of the spots elicited by the stimuli before simplification. We examined 12 pairs of activation patterns elicited by the original and the simplified stimuli, and found that five pairs (42%) showed similar results.

Interestingly, in addition to the disappearance of spots, there were also cases where new spots emerged by the simplification of an object (Fig. 5.5). For example, in Fig. 5.5a, spots A and B disappeared but spot C appeared when stimulus **1** was simplified to stimulus **3**. Similarly in Fig. 5.5b, spot A was only activated by the simplified stimulus. Among the twelve pairs, the emergence of spots by simplification was observed in seven pairs (58%) (two cases showed only emergence and five cases showed both emergence and disappearance).

To identify the visual feature represented by each spot and also to find reasons for emergence of activity spots with stimulus simplification, we recorded single cellular activities from neurons in spots shown in Fig. 5.5a (Fig. 5.6). Cells in spots A and B were significantly activated by the "handle and hose" in isolation (Fig. 5.6a-1, b-1). This result is consistent with optical response patterns elicited by stimuli 1 and 3 (Fig. 5.5a). In addition, the cells in spot A were activated by the "handle" (Fig. 5.6a-2) having protrusions, but not by the "hose" (Fig. 5.6a-3). Furthermore, other stimuli with sharp protrusions, such as a "hand" (Fig. 5.6a-4) and "cat's head" (Fig. 5.6a-5), also activated the cells. These cells seemed to require a generic visual feature, "sharp protrusions," for activation. In contrast, the cells in spot B were activated by the "hose" (Fig. 5.6b-3), but neither by the "handle" (Fig. 5.6b-2) nor by a "line segment" (Fig. 5.6b-4). We also found no activation was elicited by a segment of a circle (Data not shown). The critical feature of these cells was, thus, an "asymmetric arc."

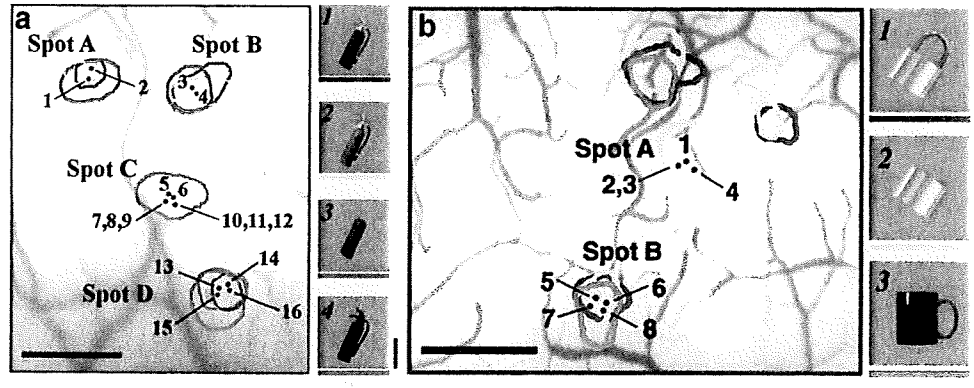

Fig. 5.5 Stimulus simplification causes appearance of new spots. The numbers indicate electrode penetration sites. (see Tsunoda et al. 2001 for electrode recordings in b) (Modified from Tsunoda et al. (2001))